6.1 Introduction

In chapters 3 and 4, we have observed interesting properties in the Cu doped Bi_2Te_3 samples. Sb_2Te_3 is one of the interesting member of an A_2B_3 family, therefore doping of Cu in Sb_2Te_3 sample might be a matter of interest and hence in this chapter we have studied the Cu doping effect in Sb_2Te_3 sample. The delocalized surface states (SS) in topological insulator remain unaffected from nonmagnetic dopants and defects and their excitation spectrum within the bulk energy gap exhibits the characteristic Dirac dispersion because of this time reversal symmetry. These surface states have been well investigated by surface sensitive techniques like (spin-) angular resolved photo-emission spectroscopy [1, 81] and scanning tunneling microscopy [116]. Such techniques describe well the electronic properties of the surface states but cannot account for other interesting transport features as observed in (magneto) transport experiments. In fact, magneto-transport measurements are frequently used to have information about the details of the Fermi surface of both bulk and surface states. Quantum oscillations of the conductivity (Shubnikov–de Haas, SdH) have their origin in the Landau level splitting of electron orbits in magnetic fields. For bulk carriers, the characteristic SdH oscillation frequencies provide information about the Fermi surface and their dependence on the orientation of the magnetic field probes the shape of the Fermi surface. For surface carriers the SdH oscillation frequencies depend on the field component normal to the surface. Furthermore, the Dirac character of the surface carriers can be shown by evaluating the temperature and field dependence of the SdH oscillations and by extracting the Berry phase.

Although Shubnikov–de Haas (SdH) oscillations are a powerful means to distinguish between bulk and surface charge carriers via their angle dependence but their analysis and

interpretation remain controversial. It is emphasized by different groups the difficulty in distinguishing between the bulk surface state (SS) and a two dimensional charge-accumulation layer [117-123]. Apart from the SS, the electronic bulk states in TIs are also of particular interest as their spin splitting is found to be twice the cyclotron energy observed in quantum oscillation [123-124]. On the other hand, The de-Haas van Alphen (dHvA) oscillation studies prove a direct way to probe in detail the bulk, full three dimensional Fermi surface and can also resolve the strength of the many body interactions at the Fermi level. Moreover, for the case of Topological Insulators surface states are not magnetic. Therefore, from the magnetization measurement we will mainly observe the bulk property. As a matter of fact, from both the SdH and dHvA oscillations the bulk and surface states in TIs can be distinguished without any angle dependent measurements. In the present study, we have shown the existence of both surface and bulk states simultaneously from the SdH and dHvA oscillations in $Sb_{1.90}Cu_{0.10}Te_3$.

6.2 Results and Discussion

6.2.1 Hall Analysis

Variation of Hall resistivity as a function of applied magnetic fields at different temperatures for $Sb_{1.90}Cu_{0.10}Te_3$ has been shown in Fig.6.1. The positive slope of the curve is showing that carriers are *p* type for the entire range of temperature of measurement. The calculated carrier concentration from Hall data at low field was 1.34×10^{21} cm^{-3} which is consistent to the reported values in pure Sb_2Te_3 [126, 127]. We have also determined the mobility (μ) of the carriers from the Hall data. Observed mobility as function of temperature is shown in the inset (a) of Fig. 6.1 whereas variation of mobility as a function of applied field at 2K and 300K is shown in inset (b) of Fig.6.1. The value of mobility is around

150cm^2/VS at 2K which well matched with the reported values in Sb_2Te_3 [127]. It is observed that as we increase both the temperature and field, mobility decreases which might be due to the freezing out of phonons with decrease of temperature and also with the increase of magnetic field. It is observed that carrier density was increasing with temperature which might be due to the fact that at high temperature bulk contribution dominates over surface contribution causing the enhancement in carrier concentration.

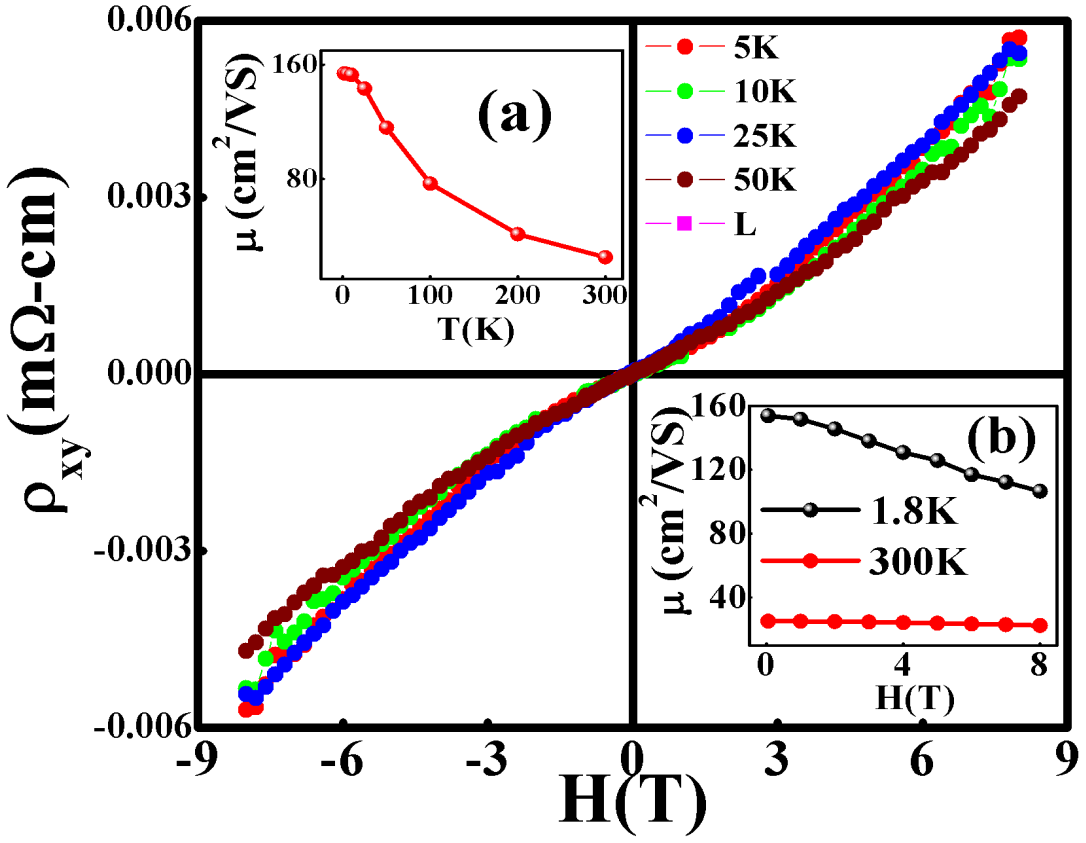

Fig.6.1 Magnetic field dependence of the Hall resistivity of $Sb_{1.90}Cu_{0.10}Te_3$ at different temperatures. Inset (a) represents the variation of carrier mobility as a function of temperature, Inset (b) Magnetic field dependence of the Hall mobility at 1.8K and 300K.

In fact, topological surface state is a complete quantum phenomenon and as a matter of fact, surface effect will be significant at very low temperature. In consequence, at very low temperature surface state dominates over bulk state and that is why the carrier concentration is low at low temperature (T≤20K) and very large at high temperature. Moreover, the rate of

increment of carrier density is also increasing with the increase of temperature confirming the dominance of bulk insulating character over surface metallic character at higher temperature.

6.2.2 Analysis of Shubnikov–de Haas (SdH) oscillation

The variation of resistivity as a function of temperature of $Sb_{1.90}Cu_{0.10}Te_3$ sample is shown in the inset of Fig. 6.2(a). The graph is showing positive slope indicating their metallic behavior. The magneto-resistance (MR) as a function of a magnetic field at different temperatures of $Sb_{1.90}Cu_{0.10}Te_3$ has been shown in Fig. 6.2(a). We have applied the magnetic field along the perpendicular direction of the applied electric current. We have defined MR as $[\rho(H)-\rho(0)]/\rho(0)*100\%$. In Fig. 6.2(a), It was obvious that resistivity value was increasing with increase in magnetic field. Large linear MR (nearly 45%) at low temperature has been shown by the sample but with increase of temperature MR was decreasing as increase of the carrier concentration lead to decrease in MR. For a high magnetic field, Landau-level induced SdH oscillations were observed at low temperatures. Quantum oscillations are clearly visible in the second derivative $-d^2\rho_{xx}/dB^2$, as a function of the inverse field as shown in Fig. 6.2(b). We have already mentioned that we have measured the MR at perpendicular magnetic field configuration only. Several frequencies are found in this perpendicular field measurement. In order to identify the origin of the quantum oscillations, we have performed fast Fourier transforms (FFTs). It was clear from Fig.6.2(c) that three frequencies has been observed. Among three frequencies one was for bulk and two were for the surface states. Taking the Onsager relation, i.e., the extremal cross section of the Fermi surface $A(E_F)=4\pi^2e/hF$ (F is the frequency) and assuming a spherical pocket we have calculated the

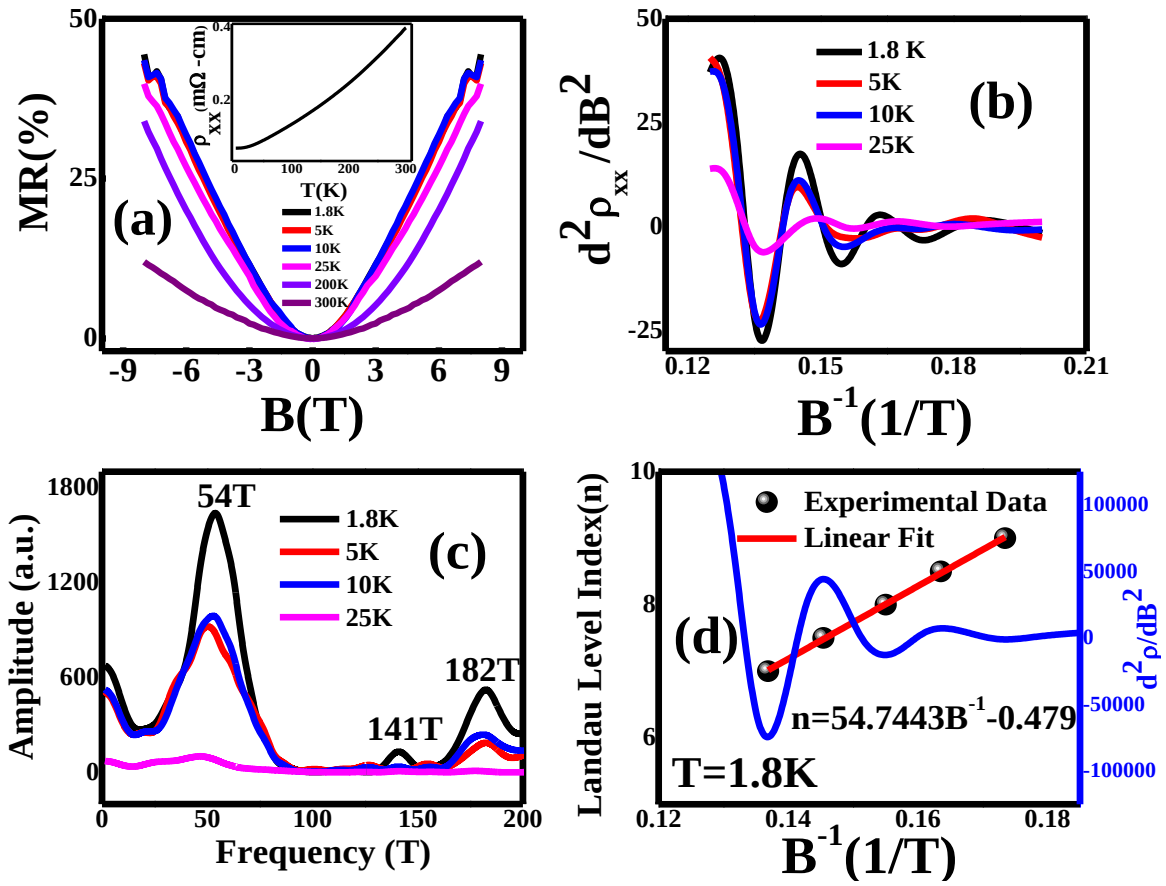

Fig.6.2 (a) Magnetoresistance $=\frac{R(H)-R(0)}{R(0)}X100\%$ as a function of magnetic field of $Sb_{1.90}Cu_{0.10}Te_3$ at different temperatures. Inset: variation of electrical resistivity with respect to Temperature. (b) SdH oscillations of the longitudinal resistance (second derivative) with 1/B at different temperatures. (c) The FFT corresponding to Fig. (b); (d) SdH oscillations (second derivative) and Landau levels with inverse magnetic field and linear fitted curve (red line).

n_{bulk} for the bulk band corresponding to the pocket with the lowest frequency for the sample. For the surface states, we have also estimated the carrier densities. All the bulk and surface carrier densities obtained from SdH oscillation are shown in Table 6.1. From the quantum oscillation analysis, we have also calculated the total carrier concentration of $n_{tot,}^{SdH}$ (given in Table 6.1) which is also consistent with those already reported [128]. The slope obtained from Landau-level fan diagram (Landau index vs. 1/B, B being the magnetic field) in Fig. 6.2(d) reflects a 2D electron density of n= (e/h)BF. Additionally, the Landau level fan

diagram was showing an intercept at ~-0.47, indicating that the Dirac fermions dominate the transport properties due to the additional Berry phase π.

Moreover, from Onsagar's relation f= $h/2\pi(2e)k^2_F$, the obtained Fermi momentum corresponds to $k_F=3.2\times10^8$ m^{-1}. The higher value of the Fermi wave vector k_F in $Sb_2Te_{2.85}Cu_{0.15}$ indicates the significant difference in the positions of the Fermi energy and Dirac point. We have also determined the cyclotron mass from the temperature dependence of the oscillations which are observable up to ~25 K as shown in Fig.6.2. We have obtained the oscillation amplitude from the different peaks of $d^2\rho/dB^2$ for different temperatures (viz. 2K, 5K, 10K and 25K) at a constant magnetic field (viz.7.32T, 6.88T and6.47T). Thermal damping factor of Lifshitz-Kosevich (LK) equation $R_T = (\frac{2\pi^2 k_B T\, m_{cyc}}{e\hbar B})/\sinh(\frac{2\pi^2 k_B T\, m_{cyc}}{e\hbar B})$ has been fitted to obtain the cyclotron mass (m_{cyc}) at different fields mentioned above. The obtained m_{cyc} respectively for 7.32T, 6.88T and 6.47T were $0.06m_0$, $0.10m_0$, $0.16m_0$. using these m_{cyc} values, we have obtained the average cyclotron mass which was found to be m_{cyc} $=0.11m_0$, where m_0 is the rest mass of an electron. Comparing this result with the FFT spectrum evolution in Fig.6.2(c), we have found a single channel up to ~54T. We observed that the peak for cyclotron mass m_c $=0.06m_e$ corresponds to this channel which is consistent with the bulk conduction band [129]. The enhancement of cyclotron mass below the $0.06m_e$ peak might be due to the topological surface states [130] whereas a trivial 2 dimentional electron gas (2DEG) is supposed to have a similar mass as the bulk [131]. The interplay of the different oscillations could give rise to an increase in the cyclotron mass because of the contribution of lower mobility channels [132].

Using the linear dispersion relation for the surface state $v_F= hk_F/2\pi m_c$, we have estimated the Fermi velocity $v_F=4.3\times10^5 ms^{-1}$. Following the standard Dingle temperature

analyses (Fig.6.3), we have calculated the Dingle temperature, T_D= 36.8K and with the help of this value in the expression $\tau=h/4\pi^2K_BT_D$, the estimated surface carrier life time was 3.3×10^{-14}s. Similarly, we have also estimated the mean free path $l = v_F\tau$, mobility $\mu=e\tau/m_{cyc}$, and Fermi energy E_F to be 14nm, 313cm^2/Vs, and 115 meV, respectively. These physical parameters were found to be consistent to those already reported on other topological systems [47].

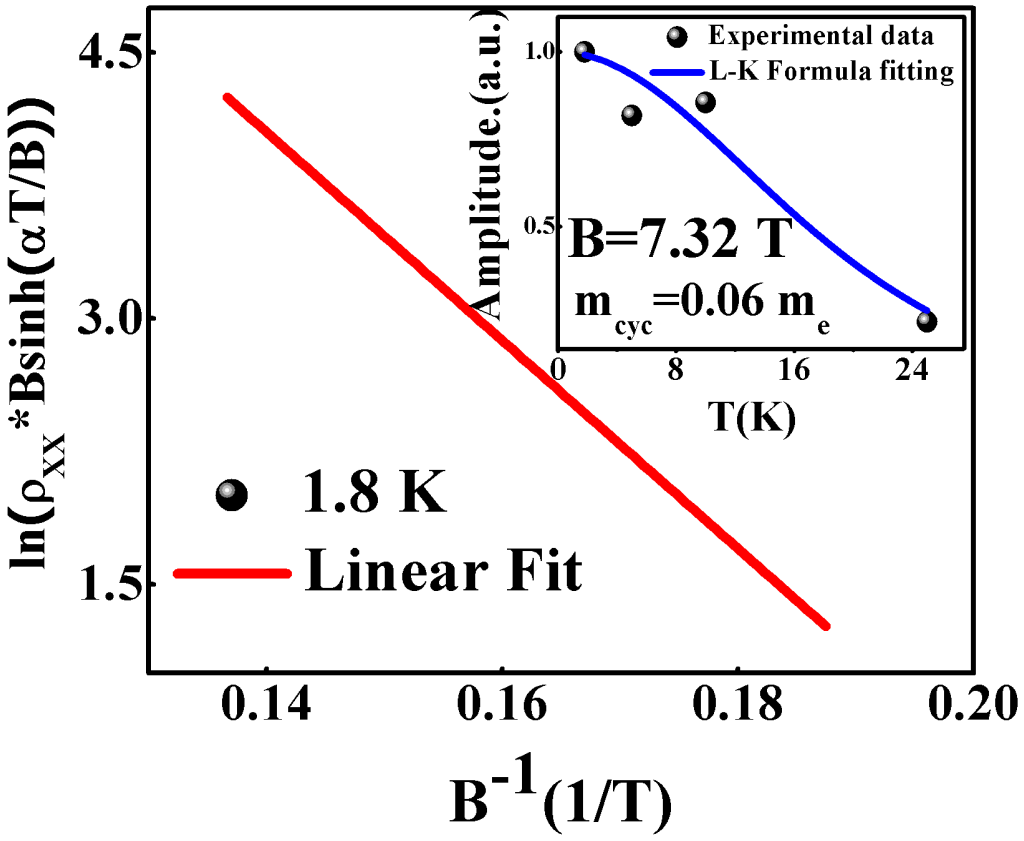

Fig.6.3 Fit to the Dingle damping term at 1.8K with the resulting Dingle temperature T_D=36.8K, Inset show the L-K fitting of the SdH oscillation and obtained cyclotron mass (m_c) from fitting at applied field 7.32T.

6.2.3 Analysis of The de-Haas van Alphen (dHvA) oscillation

In order to find the magnetic field effect on magnetization we have also measured the variation of magnetization as a function of magnetic field as well as temperature shown in fig. 6.4(a) and its inset respectively. In Fig. 6.4(a), we have observed that magnetization was

increasing with increase in magnetic field. For a higher magnetic field, Landau-level induced de-Has van Alphen (dHvA) oscillations were observed at low temperatures. We have plotted the quantum oscillations (similar to the transport case) in the second derivative $-d^2M/dB^2$, as a function of the inverse field [shown in fig. 6.4(b)]. We have also performed fast Fourier transforms (FFTs) to identify the origin of the oscillations. It is clear from fig.6.4(c) that only

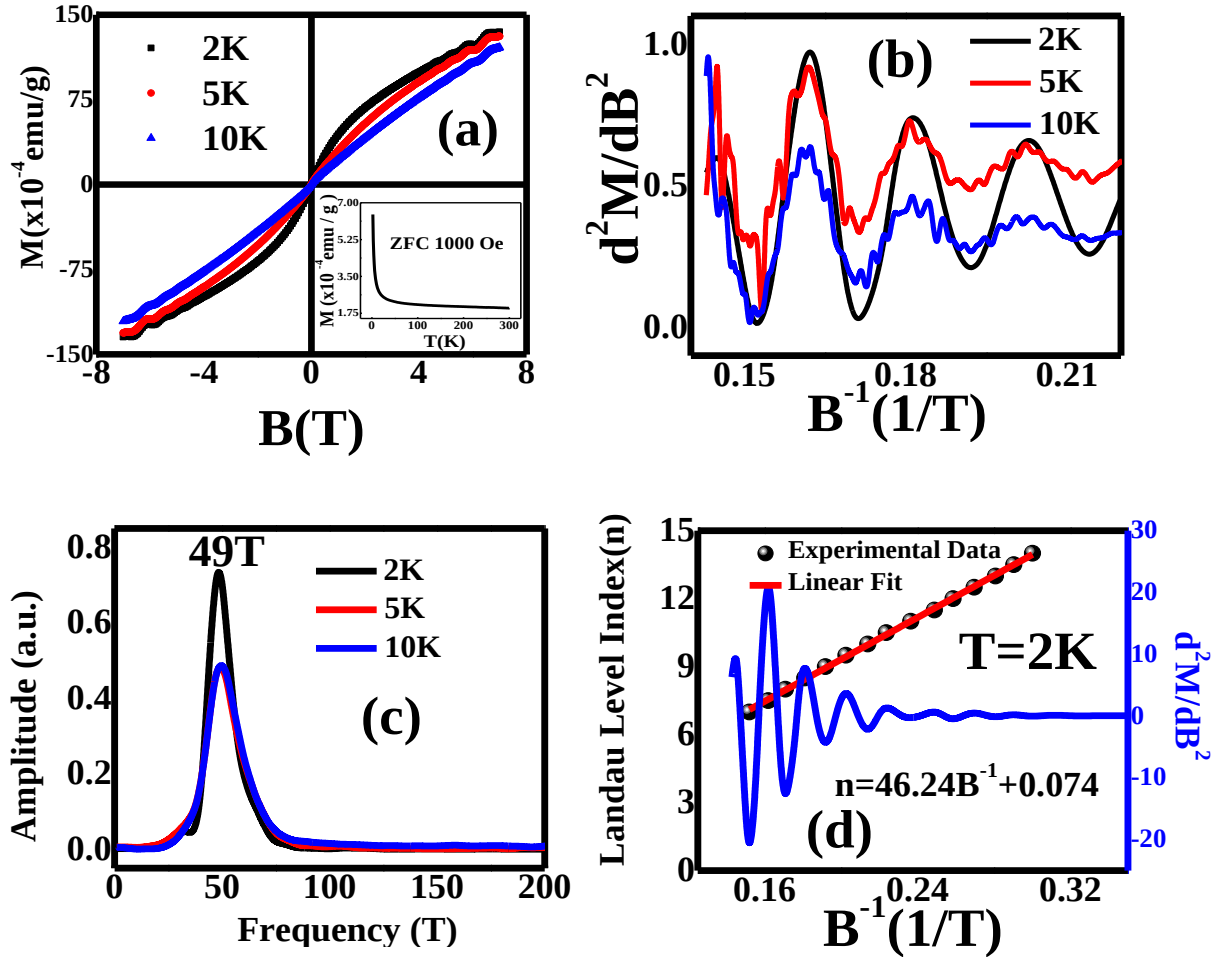

Fig.6.4 (a) Field dependence of magnetization of $Sb_{1.90}Cu_{0.10}Te_3$ at 2K, 5K and 10K respectively. The inset represents Temperature dependence of magnetization in ZFC mode at an applied magnetic field of 1000 Oe. (b) SdH oscillations in the magnetization (second derivative) with 1/B at different temperatures. (c) The FFT corresponding to Fig. (b), (d) dHvA oscillations of the magnetization (second derivative) and Landau levels with inverse magnetic field and linearly fitted data red line).

one prominent frequency is observed at 49T. This frequency is comparable to that observed for bulk state in transport measurement. Similar to the transport case, taking the Onsager relation of the Fermi surface $A(E_F)=4\pi^2e/hF$ and assuming a spherical pocket we have

calculated the n_{bulk}^{dHvA} (shown in Table 6.1).The calculated n_{bulk}^{dHvA} is consistent to that calculated from resistivity (n_{bulk}^{SdH}) data but different from that determined from Hall effect (n^{Hall}). The difference is might be due to the position of the Fermi energy at deep inside the valence band which is also supported by the value of k_F estimated from the transport data. We have also plotted the Landau level Fan diagram of the present dHvA oscillation as shown in Fig. 6.4(d). The obtained intercept is ~0.074 (close to zero) implying the existence of normal fermions. This clearly indicates the contribution is from bulk state only.

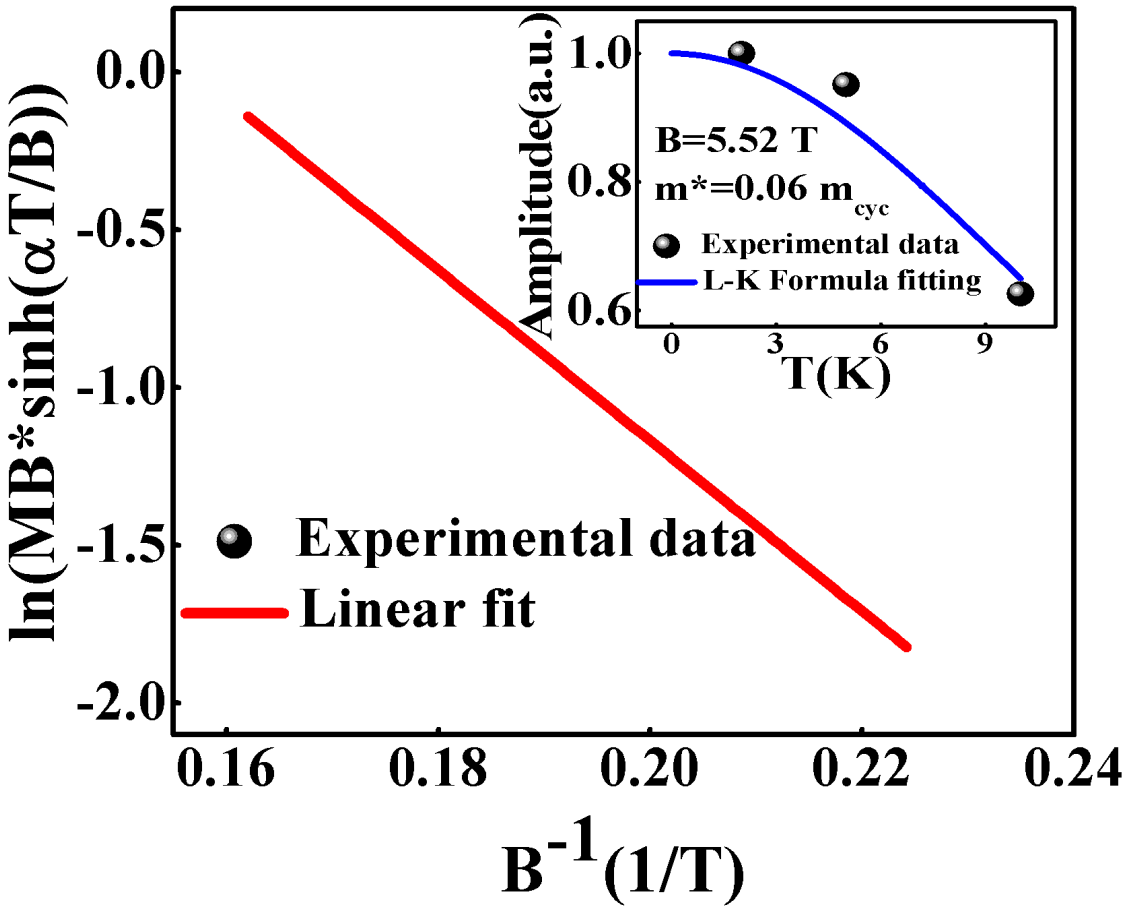

Fig.6.5 Fit to the Dingle damping term at 1.8K with the resulting Dingle temperature T_D=29.3K, Inset shows the L-K fitting of the dHvA oscillation in magnetization and obtained cyclotron mass (m_{cyc}) from fitting at applied field 5.52T.

As we have already mentioned in the analysis of transport measurement that from the determination of cyclotron mass one can have idea regarding the origin of the states, we have also extracted the same in this case (shown in inset of Fig. 6.5). It is observed that the estimated cyclotron mass from n_{bulk}^{dHvA} is 0.06 m_e which well matched with the value obtained for the bulk state from the SdH oscillation. We have also determined different physical parameters from the Dingle temperature analyses (Fig.6.5). The obtained Dingle temperature, T_D= 29.3K and corresponding carrier lifetime was 4.2×10^{-14}s. The calculated mean free path *l*, mobility μ and Fermi energy E_F is found to be 29 nm, 1162cm^2/Vs and 180 meV respectively. These physical parameters are different from those obtained from SdH oscillation which might be due to the contribution of surface state in magneto-transport.

Table-6.1: Different parameters (**k_F,** the Fermi momentum**;** **n_b**, the bulk carrier concentration**;** **n_s**, the surface carrier concentration**;** **n_{tot},** the total carrier concentration**)** obtained from SdH, dHvA oscillations and their first Fourier transforms**.**

From SdH Oscillation	**From dHvA Oscillation**	**From SdH Oscillationfor different FFT peak**
(From slope 54.74) **k_F**=3.2×10^8 m^{-1} **n_b**=1.14×10^{18}cm^{-3}	(From slope 46.24) k_F=9.2×10^8m^{-1} **n_b**=2.66×10^{18}cm^{-3}	F=54T, k_F=4.1×10^8m^{-1},**n_b**=2.24×10^{18}cm^{-3} F=141T, **n_s**=3.4×10^{12}cm^{-2} F=182T, **n_s**=4.3×10^{12}cm^{-2},
From Hall data **n_b**=1.34×10^{21}/cm^3	**FFT peak F=49T** k_F=3.9×10^8 m^{-1} **n_{tot}^{dHvA}**=1.94×10^{18}cm^{-3}	n_{tot}^{SdH}=2.24×10^{18}cm^{-3}

6.3 Conclusion:

In summery we have measured the magneto-transport and magnetization at different temperatures and different fields. The coexistence of both bulk and surface states were seen from SdH oscillation. But from the dHvA oscillation we observed only the existence of bulk state. It is due to the fact that non magnetic Cu doping induces the magnetic ordering and

induced magnetization is the bulk property. Therefore, the bulk state can be distinguished from the surface state in this $Sb_{1.90}Cu_{0.10}Te_3$ from the simultaneous measurements of magneto-transport and magnetization at high field and low temperature.